doi:10.1093/brain/awaa249 BRAIN 2020: 143; 2973–2987 | 2973

BRAIN
A JOURNAL OF NEUROLOGY

7 T imaging reveals a gradient in spinal cord lesion distribution in multiple sclerosis

Russell Ouellette,[1,2,3] Constantina A. Treaba,[1,4] Tobias Granberg,[1,2,3,4] Elena Herranz,[1,4] Valeria Barletta,[1,4] Ambica Mehndiratta,[1] Benjamin De Leener,[5] Shahamat Tauhid,[4,6] Fawad Yousuf,[4,6] Sarah M. Dupont,[7] Eric C. Klawiter,[4,8] Jacob A. Sloane,[4,9] Rohit Bakshi,[4,6] Julien Cohen-Adad[7] and Caterina Mainero[1,4]

We used 7 T MRI to: (i) characterize the grey and white matter pathology in the cervical spinal cord of patients with early relapsing-remitting and secondary progressive multiple sclerosis; (ii) assess the spinal cord lesion spatial distribution and the hypothesis of an outside-in pathological process possibly driven by CSF-mediated immune cytotoxic factors; and (iii) evaluate the association of spinal cord pathology with brain burden and its contribution to neurological disability. We prospectively recruited 20 relapsing-remitting, 15 secondary progressive multiple sclerosis participants and 11 age-matched healthy control subjects to undergo 7 T imaging of the cervical spinal cord and brain as well as conventional 3 T brain acquisition. Cervical spinal cord imaging at 7 T was used to segment grey and white matter, including lesions therein. Brain imaging at 7 T was used to segment cortical and white matter lesions and 3 T imaging for cortical thickness estimation. Cervical spinal cord lesions were mapped voxel-wise as a function of distance from the inner central canal CSF pool to the outer subpial surface. Similarly, brain white matter lesions were mapped voxel-wise as a function of distance from the ventricular system. Subjects with relapsing-remitting multiple sclerosis showed a greater predominance of spinal cord lesions nearer the outer subpial surface compared to secondary progressive cases. Inversely, secondary progressive participants presented with more centrally located lesions. Within the brain, there was a strong gradient of lesion formation nearest the ventricular system that was most evident in participants with secondary progressive multiple sclerosis. Lesion fractions within the spinal cord grey and white matter were related to the lesion fraction in cerebral white matter. Cortical thinning was the primary determinant of the Expanded Disability Status Scale, white matter lesion fractions in the spinal cord and brain of the 9-Hole Peg Test and cortical thickness and spinal cord grey matter cross-sectional area of the Timed 25-Foot Walk. Spinal cord lesions were localized nearest the subpial surfaces for those with relapsing-remitting and the central canal CSF surface in progressive disease, possibly implying CSF-mediated pathogenic mechanisms in lesion development that may differ between multiple sclerosis subtypes. These findings show that spinal cord lesions involve both grey and white matter from the early multiple sclerosis stages and occur mostly independent from brain pathology. Despite the prevalence of cervical spinal cord lesions and atrophy, brain pathology seems more strongly related to physical disability as measured by the Expanded Disability Status Scale.

1 Athinoula A. Martinos Center for Biomedical Imaging, Department of Radiology, Massachusetts General Hospital, Charlestown, MA, USA
2 Department of Clinical Neuroscience, Karolinska Institutet, Stockholm, Sweden
3 Department of Radiology, Karolinska University Hospital, Stockholm, Sweden
4 Harvard Medical School, Boston, MA, USA
5 Department of Computer Engineering and Software Engineering, Polytechnique Montreal, Montreal, QC, Canada
6 Brigham and Women's Hospital, Boston, MA, USA
7 NeuroPoly Lab, Institute of Biomedical Engineering, Polytechnique Montreal, Montreal, QC, Canada
8 Department of Neurology, Massachusetts General Hospital, Boston, MA, USA
9 Beth Israel Deaconess Medical Center, Boston, MA, USA

Received December 16, 2019. Revised June 3, 2020. Accepted June 29, 2020. Advance access publication September 16, 2020

Correspondence to: Caterina Mainero MD, PhD
A.A. Martinos Center for Biomedical Imaging, Massachusetts General Hospital
Department of Radiology, Harvard Medical School, Room 2301, Building 149, 13th Street
Charlestown, MA 02129, USA
E-mail: cmainero@mgh.harvard.edu

Keywords: multiple sclerosis; imaging; biomarkers; white matter lesions; demyelination

Abbreviations: 9-HPT = 9-Hole Peg Test; EDSS = Expanded Disability Status Scale; RRMS = relapsing-remitting multiple sclerosis; SPMS = secondary progressive multiple sclerosis

Introduction

Spinal cord lesions and atrophy are established components of multiple sclerosis pathology and key contributors to disability and disease progression (Agosta *et al.*, 2007; Eden *et al.*, 2019). It is evident from neuropathological examinations that, similar to the brain, the grey and white matter of the spinal cord can be affected by inflammation, demyelination, and neuroaxonal degeneration (Oppenheimer, 1978; Gilmore *et al.*, 2006, 2009; Lucchinetti *et al.*, 2011). Previous histopathological and neuroimaging multiple sclerosis studies have demonstrated the presence of an outside-in pathological gradient in the brain, expressed in both the grey and white matter, with the most marked abnormalities seen in the immediate CSF-surface brain regions. These include the periventricular white matter (Liu *et al.*, 2015; Brown *et al.*, 2017) and subpial cortical layers bordering meningeal inflammation (Magliozzi *et al.*, 2010; Mainero *et al.*, 2015). These findings have been interpreted as consistent with the outside-in theory of CSF-/ependymal-mediated inflammatory pathogenesis for demyelination in multiple sclerosis (Adams *et al.*, 1987; Magliozzi *et al.*, 2010).

Early neuropathological examinations in multiple sclerosis suggest that the predilection of lesion origin and expansion in periventricular brain regions could be induced by a causative disease agent entering the parenchyma via the CSF (Dawson, 1916; Fog, 1965; Lumsden *et al.*, 1970). This was later elaborated after lymphocytic infiltrates in the parenchyma were identified to be of a subependymal perivenular origin (Adams *et al.*, 1987). Subsequent post-mortem examination has also identified meningeal inflammation with B-lymphocytes to be topographically associated with cortical demyelinating lesions (Magliozzi *et al.*, 2010). A fundamental feature of the outside-in pathogenic mechanism is that the penetrating lymphocytes (T and B cells) do not directly interact with the end target cells, but rather produce soluble factors that either diffusely destroy tissue and/or activate microglia or macrophages to mediate more focal tissue damage (Kutzelnigg and Lassmann, 2006; Magliozzi *et al.*, 2010; Lassmann, 2019). In the spinal cord, neuropathological studies of progressive multiple sclerosis have identified meningeal inflammation in association with axonal loss and demyelination (Androdias *et al.*, 2010; Gass *et al.*, 2015). This observation, however, has yet to be verified *in vivo*, and the development of spinal cord pathology in earlier multiple sclerosis disease stages still remains uncertain. The pattern of lesion distribution throughout the spinal cord and brain may, therefore, shed further light on the pathogenic development of the disease and possibly implicate routes of immune penetrance into the CNS.

MRI is the most sensitive preclinical tool to identify brain and spinal cord multiple sclerosis pathology *in vivo* (Thompson *et al.*, 2018). This pathological sensitivity is increased at higher field strengths where the increased signal-to-noise and contrast-to-noise allows for small and subtle lesions to be identified (Mainero *et al.*, 2009; Dula *et al.*, 2016; Kilsdonk *et al.*, 2016). Spinal cord MRI is technically challenging since the structure itself is narrow, mobile and flexible (Stroman *et al.*, 2014; Kearney *et al.*, 2015*a*; De Leener *et al.*, 2017; Muccilli *et al.*, 2018). The smaller volume of lesions therein necessitates the demand for increased spatial resolution (Barry *et al.*, 2018). In this study, in a cohort of subjects with either relapsing-remitting or secondary progressive multiple sclerosis (RRMS, SPMS), we used ultra-high field 7 T MRI to (i) characterize the extent of grey and white matter lesions and atrophy in the cervical spinal cord; (ii) evaluate whether spinal cord lesions preferentially occur in close proximity to CSF surfaces, possibly implying an association with CSF-mediated inflammatory factors; and (iii) investigate the relationship between brain and spinal cord pathology and their relative contributions to neurological disability.

Materials and methods

Study population and clinical assessments

Our Institution Ethics Committee approved all study procedures and written informed consent in accordance with the Declaration of Helsinki was obtained from all participants before study enrolment. We prospectively enrolled 35 individuals with multiple sclerosis (20 RRMS, 15 SPMS) diagnosed according to the 2010 McDonald criteria (Polman *et al.*, 2011) and meeting the following inclusion criteria: age between 18 to 65 years; being on stable disease-modifying treatment or not receiving treatment for at least 3 months; absence of clinical relapse(s) within the preceding 3 months and no corticosteroid use within a month prior to study enrolment. All RRMS participants had a disease duration within 5 years and thus classified in the early stage of the disease. We also recruited 11 age- and gender-

matched healthy volunteers [five females, mean ± standard deviation (SD) age 43.5 ± 9.1 years] as controls. General exclusion criteria were: MRI contraindications, significant medical history or comorbidities, and/or neurological disease (beyond multiple sclerosis). A detailed description of the study population demographics can be found in Table 1. Neurological disability in multiple sclerosis participants was assessed using the Expanded Disability Status Scale (EDSS) (Kurtzke, 1983), the 9-Hole Peg Test (9-HPT) and Timed 25-Foot Walk within a week from the imaging procedures.

Image acquisition and analysis

Representative examples of spinal cord and brain images at 7 T are provided in Fig. 1. The image processing pipeline is detailed below and illustrated in both Figs 2 and 3 for the spinal cord and in Fig. 4 for the brain.

MRI acquisition

All participants underwent brain and spinal cord imaging on a 7 T MAGNETOM whole-body MRI scanner (Siemens Healthcare). Spinal 7 T imaging was performed in all study participants using a 19-channel receive array with a 4-channel transmit array coil developed in-house (Zhao *et al.*, 2014). The imaging protocol consisted of axial and sagittal 2D multi-echo fast low-angle shot (FLASH) T_2*-weighted spoiled gradient-echo sequences (axial and sagittal: repetition time = 500 ms, echo times = 7.8, 13.73, 18.42 ms, flip angle = 55°, resolution = 0.40 × 0.40 × 3.0 mm^3, bandwidth = 430 Hz/pixel; axial: slabs of 18 slices, field of view = 220 × 73 mm^2, acquisition time for each slab = ∼2 min; sagittal: slabs of 11 slices, field of view = 220 × 222 mm^2, acquisition time for each slab = ∼2 min). Axial acquisitions were aligned perpendicularly to the spinal cord curvature for the respective field of view, aiming to best mitigate partial volume effects. Depending upon the degree of natural spinal curvature, two or three axial slabs were used to maintain perpendicular alignment (Fig. 2A) across the entire cervical spinal cord (C1 to C7). All participants received coaching to mitigate bulk movement and lessen physiological noise such as swallowing, respiration and lingual movement (Kearney *et al.*, 2015*a*).

Brain 7 T imaging was performed in 29 of 35 multiple sclerosis participants and all control subjects using a custom-built 32-channel phased-array head coil to acquire a 2D single-echo FLASH T_2*-weighted spoiled gradient-echo pulse sequence (repetition time/echo time = 1700/21.8 ms, two slabs of 40 slices each to cover the supratentorial brain, field of view = 192 × 168 mm^2, resolution = 0.33 × 0.33 × 1.0 mm^3, bandwidth = 335 Hz/pixel, acquisition time for each slab = ∼8 min) for cortical lesion segmentation. All participants were also scanned on the 3 T MGH-USC Skyra CONNECTOM scanner (Siemens Healthcare) using a custom-made 64-channel head coil to acquire a structural brain scan with a 3D T_1-weighted multi-echo magnetization-prepared rapid gradient-echo sequence (MEMPRAGE: repetition/inversion/echo times = 2530/1100/1.15, 3.03, 4.89, 6.75 ms, flip angle 7°, field of view = 230 × 230 mm^2, resolution 1.0 × 1.0 × 1.0 mm^3, bandwidth 651 Hz/pixel, acquisition time = ∼6 min) used for cortical surface reconstruction, and cortical thickness measurements. Additionally, a 3D T_2-weighted fluid-attenuated inversion recovery (FLAIR) sequence (repetition/inversion/echo time = 5000/1800/393 ms, field of view = 2356 × 256 mm^2, resolution 1.0 × 1.0 × 1.0 mm^3, acquisition time = ∼7 min) was acquired for manual brain white matter lesion segmentation.

Spinal cord segmentation

Cervical spinal cord segmentations and cross-sectional areas were obtained using the Spinal Cord Toolbox (SCT, v3.0.1) (De Leener *et al.*, 2017), which is publicly available (https://sourceforge.net/projects/spinalcordtoolbox/). The SCT 'PropSeg' algorithm uses a support vector machine trained with a histogram of oriented gradient features algorithm to identify the centre of the spinal cord (Gros *et al.*, 2018), then applies a deformable model to propagate the tubular surface along the spinal cord edge (De Leener *et al.*, 2014). Tissue volumes (grey and white matter) were then obtained through registration to the PAM50 template (De Leener *et al.*, 2018) and isolation using a multi-atlas template-based approach (Dupont *et al.*, 2017), aided by the inherent image contrast of the T_2^*-weighting. Axial spinal images were used as input for the grey and white matter tissue segmentation, while the sagittal spinal sequences were used to manually identify the cervical levels. Cervical spinal cord cross-sectional areas (mm^2) for both grey and white matter were automatically calculated in SCT at the C2–C3 level.

Brain segmentation

Cortical surface reconstruction was generated using the 3 T T_1-weighted (MEMPRAGE) images as input for FreeSurfer (v. 5.3.0, http://freesurfer.net) (Fischl, 2012). White matter hypo-intensities and topological cortical surface reconstruction defects caused by white matter and leucocortical lesions were semi-automatically corrected through lesion in-painting within the FreeSurfer processing pipeline. From these finalized reconstructions, mean cortical thickness and total intracranial volume measures were then obtained. Segmentation of the ventricular system including the choroid plexuses and the brain white matter were also obtained using FreeSurfer.

Lesion quantification

Spinal cord and brain lesions were manually segmented on the T_2*-weighted gradient-echo sequence using Slicer (v. 4.2.0, https://www.slicer.org) (Fedorov *et al.*, 2012), through the agreement of two experienced raters (C.A.T and C.M.), as previously detailed (Mainero *et al.*, 2015; Treaba *et al.*, 2019). Spinal cord lesions were segmented on the axial spinal images and confirmed in the sagittal spinal acquisition. Representative examples of spinal cord and brain lesions and segmentations are shown in Figs 1 and 2. Spinal cord lesion fractions were quantified as the proportion of lesioned tissue in grey and white matter, respectively, by combining the lesion mask with the grey and white matter segmentations from SCT.

Before manual segmentation of brain lesions, the two slabs were registered using a boundary-based registration method, into the same space as the 3 T anatomical FreeSurfer reconstructions as previously detailed (Greve and Fischl, 2009; Mainero *et al.*, 2015; Louapre *et al.*, 2018). Brain 7 T scans were discarded in 6 of 46 participants because of motion artefacts. In these cases, brain lesion segmentation was performed using a 3D T_2-weighted FLAIR acquired at 3 T. Brain lesion volumes were

Table 1 Study participant demographics and clinical characteristics

	Controls	All MS	RRMS	SPMS
Demographics				
Participants, *n*	11	35	20	15
Sex, *n*, female/male	5/6, $P = 0.12$[a]	25/10	15/5	10/5
Age, years	44.1 ± 9.3, $P = 0.40$[b]	46.9 ± 9.5	42.6 ± 8.3	52.6 ± 8.2
Disease duration, years	–	11.1 ± 11.1	3.5 ± 1.3	21.3 ± 10.2
Clinical disability metrics				
EDSS, median (range)	–	2 (0–6.5)	2 (0–3.5)	3.5 (2–6.5)
Timed 25-Foot Walk, s	–	5.3 ± 2.5	4.0 ± 0.6	7.0 ± 3.1
9-HPT, s	–	23.5 ±11.3	18.2 ± 2.0	30.4 ± 14.5
Disease-modifying therapy				
Total	–	32	17	15
Dimethyl fumarate	–	9	6	3
Glatiramer acetate	–	5	4	1
Fingolimod	–	4	1	3
Rituximab	–	4	1	3
Interferon beta-1a	–	3	3	0
Natalizumab	–	3	1	2
Teriflunomide	–	2	1	1
Mycophenolate mofetil	–	1	0	1
Ocrelizumab	–	1	0	1

[a]*P*-value versus all multiple sclerosis participants by chi-square (two-tailed).
[b]*P*-value versus all multiple sclerosis participants by unpaired two-tailed *t*-test (equal variances not assumed).
All values are given as mean ± standard deviation unless otherwise specified.
MS = multiple sclerosis.

extracted using fslstats (FMRIB Software Library, FSL, v. 5.0, Oxford, UK, http://fsl.fmrib.ox.ac.uk/fsl) (Jenkinson *et al.*, 2012).

Lesion mapping

Distance-based voxel-wise lesion segmentation was performed in the spinal cord and brain using scikit-image (version 0.14.1) NumPy and SciPy to generate a concentric layer map on the basis of distance from the CSF. In the brain, concentric dilations began at the ependymal cell lined ventricular system that is continuous with the central canal. In the spinal cord, dilations began at the inner central canal CSF surface, projecting through the central spinal cord tissue and extending to the outer subpial CSF surface (Van der Walt *et al.*, 2014; Louapre *et al.*, 2018) (Figs 2B and 3A). In the brain, dilations began at the ventricle border extending into the periventricular white matter (Fig. 4A). Concentric voxel dilations were expanded for a total of 10 layers, in widths of 2 and 4 voxels throughout the cervical spinal cord and brain (Louapre *et al.*, 2018). At comparable resolution, the layer directly bordering the CSF was previously found to be contaminated with CSF signal due to partial volume effects (Louapre *et al.*, 2018), therefore, the layer directly bordering the CSF was discarded (Kearney *et al.*, 2014; Liu *et al.*, 2015). Lesions were then mapped as a function of distance from the central canal and ventricular surfaces by extracting the dilation values from the multiple sclerosis participants' spinal cord and brain lesion segmentation using fslutils (FMRIB Software Library, FSL, v. 5.0) (Jenkinson *et al.*, 2012). To not skew the results towards those with greater lesion volume and account for the expansion of the concentric dilations, the lesion volume in each lesion dilation level was normalized first by the multiple sclerosis participant's total respective lesion volume, and second by the volume of the respective concentric dilation level both in the spinal cord and brain (Figs 3A and 4A, respectively). The resulting equation was as follows:

$$\frac{(Dilation\ level\ lesion\ volume)}{(Total\ lesion\ volume) + (Dilation\ layer\ volume)} \times 100 \quad (1)$$

This process was applied in the cervical spinal cord for the whole lesion, grey and white matter tissue compartments (Fig. 3), and for white matter lesions in the brain (Fig. 4). The process was also performed as a subgroup analysis where the rank difference between RRMS and SPMS was calculated and visualized in the cervical spinal cord and brain (Figs 3B and 4B, respectively).

Statistical analysis

Statistical analyses were performed in IBM SPSS Statistics version 24 for Mac (IBM, Armonk, USA). The normality of each variable was determined by the Shapiro-Wilk test and by evaluating the skewness and kurtosis. Group level comparisons were performed using the independent sample *t*-test for parametric data and the Mann-Whitney U-test for non-parametric data. Group level gender differences were tested between multiple sclerosis participants and control subjects using a chi-square test. Bivariate correlations between parametric variables were tested using Pearson correlation. Spearman's rank-order correlation was used in the case of non-parametric variables. Stepwise linear regression analysis of the individual clinical tests (EDSS, 9-HPT, Timed 25-Foot Walk) was done using only the respective statistically significant MRI metrics as input to determine

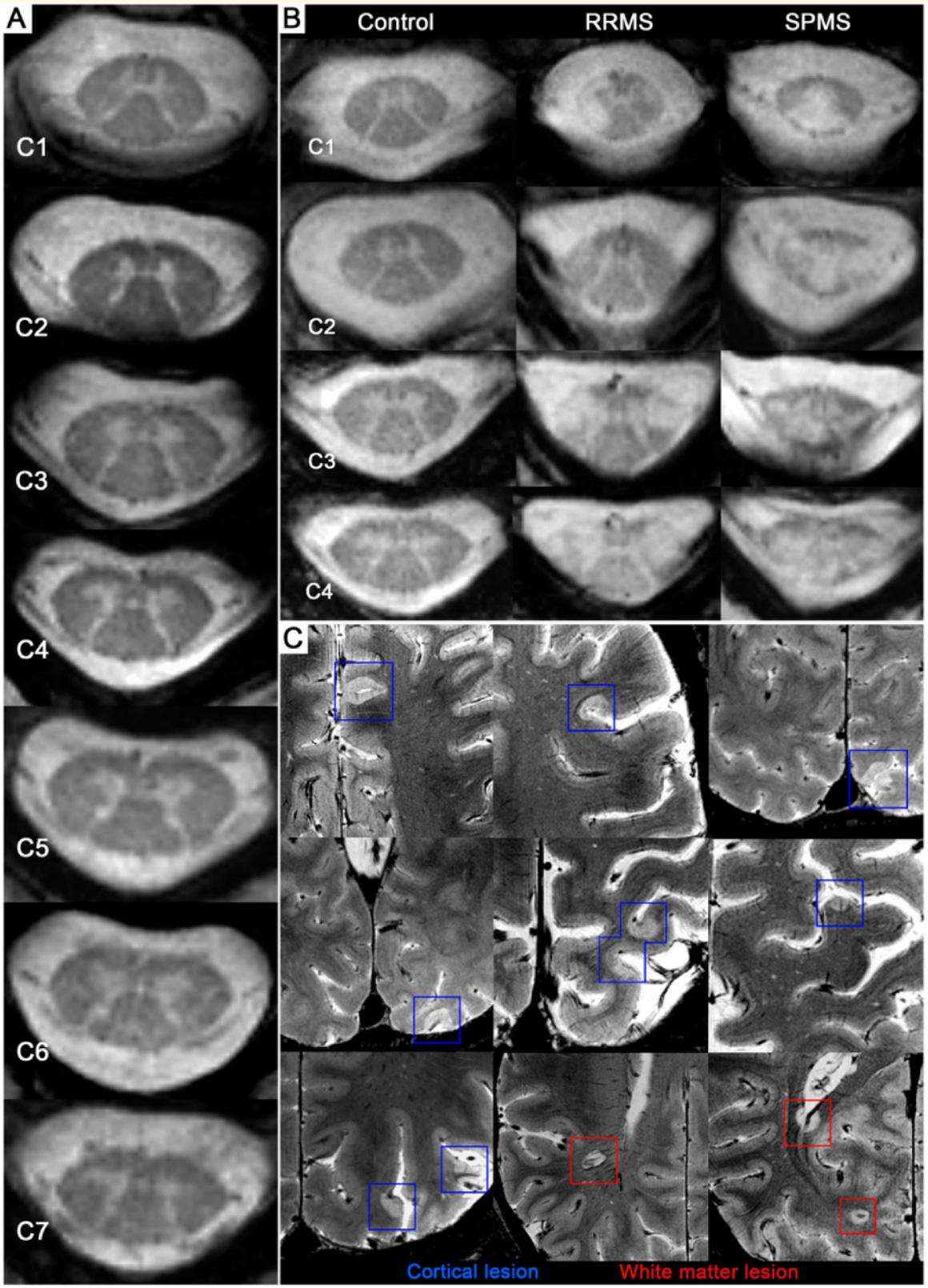

Figure 1 Ultra-high field strength MRI detection of cervical spinal cord and brain lesions. (**A**) Full coverage of the cervical spinal cord (C1–C7) in a 40-year-old female RRMS participant, disease duration of 3 years and an EDSS score of 2. (**B**) Cervical levels (C1–C4, from *left* to *right*) in a 42-year-old female healthy volunteer, 45-year-old male RRMS participant (disease duration: 4 years, EDSS: 2) and 36-year-old male SPMS participant (disease duration: 20 years, EDSS: 6.5). (**C**) Cortical (blue) and white matter (red) lesions shown in the same 45-year-old male RRMS participant.

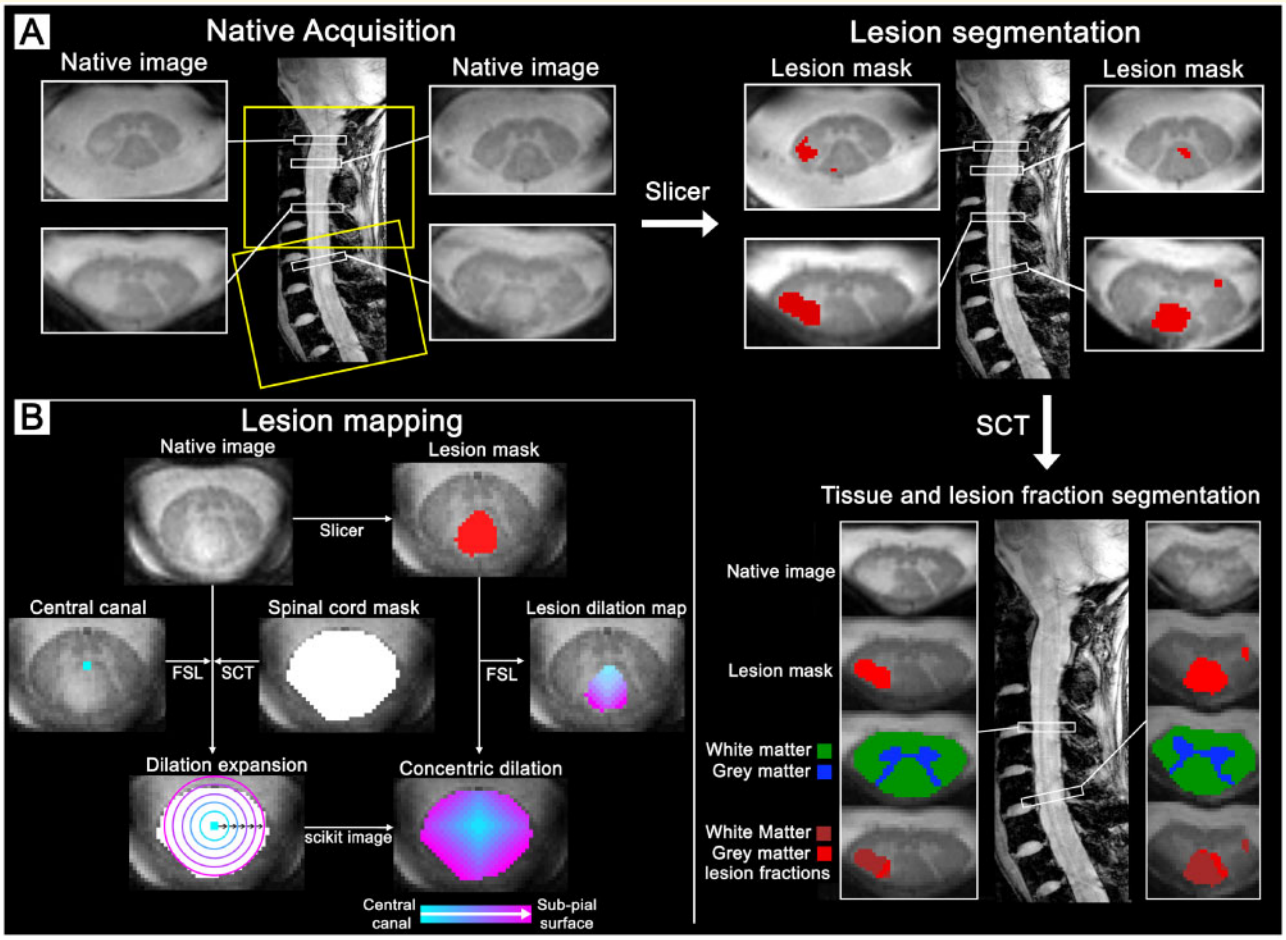

Figure 2 Image acquisition and processing pipeline for the cervical spinal cord. (**A**) Spinal cord at 7 T of a 32-year-old female (RRMS, EDSS: 2.5, disease duration: 4.8 years). Acquisition with full cervical coverage aligned orthogonally to spinal cord to mitigate partial volume effects. Spinal cord lesions were manually segmented using Slicer to then be combined with the white matter and grey matter tissue segmentations from SCT to isolate the grey matter and white matter lesion fractions. (**B**) Spinal cord lesion mapping at 7 T of a 33-year-old female (RRMS, EDSS: 1, disease duration: 2.3 years). Manual segmentation of the central canal was used as a reference from which concentric 3D voxel-wise dilations expanded radially using scikit-image towards the subpial border, as defined by the SCT spinal cord volume. The concentric lesion dilation map was created by extracting the manual lesion segmentation from the corresponding whole spinal cord concentric dilation map using FSL. FSL = FMRIB Software Library; SCT = Spinal Cord Toolbox.

which influences the respective clinical disability metric the most. For the purpose of the linear regression model, non-parametric variables were transformed, $\log_{10}$: EDSS, 9-HPT, Timed 25-Foot Walk, and square root: spinal cord lesion fractions, brain white matter lesion and cortical lesion fraction. Correction for multiple comparisons was performed using the meta-analytic software within the seed-based d mapping neuroimaging software library (http://www.sdmproject.com/utilities/? show=FDR), which is based on the work of Benjamini and Hochberg (1995). Exploratory analyses were not corrected for multiple comparisons. A P-value < 0.05 (two-tailed, equal variances not assumed) was considered statistically significant.

Data availability

Anonymized data that supported the findings of this study, not published in this article, will be shared upon a reasonable request from a qualified investigator.

Results

Characterization of demographics and clinical disability metrics

The demographics of all study participants and clinical data of multiple sclerosis subjects are detailed in Table 1.

Spinal cord and brain MRI results

The full MRI characteristics for the cohort are detailed in Table 2. Cervical spinal cord lesions were identified in 29 of 35 (83%) multiple sclerosis participants: in 14 of 20 (70%) RRMS (median 2, range 0–9 lesions) and in all 15 SPMS participants (median 4, range 2–9 lesions) with a slight trend for SPMS subjects having a higher cervical spinal cord lesion count ($P = 0.074$). Participants with multiple sclerosis had a

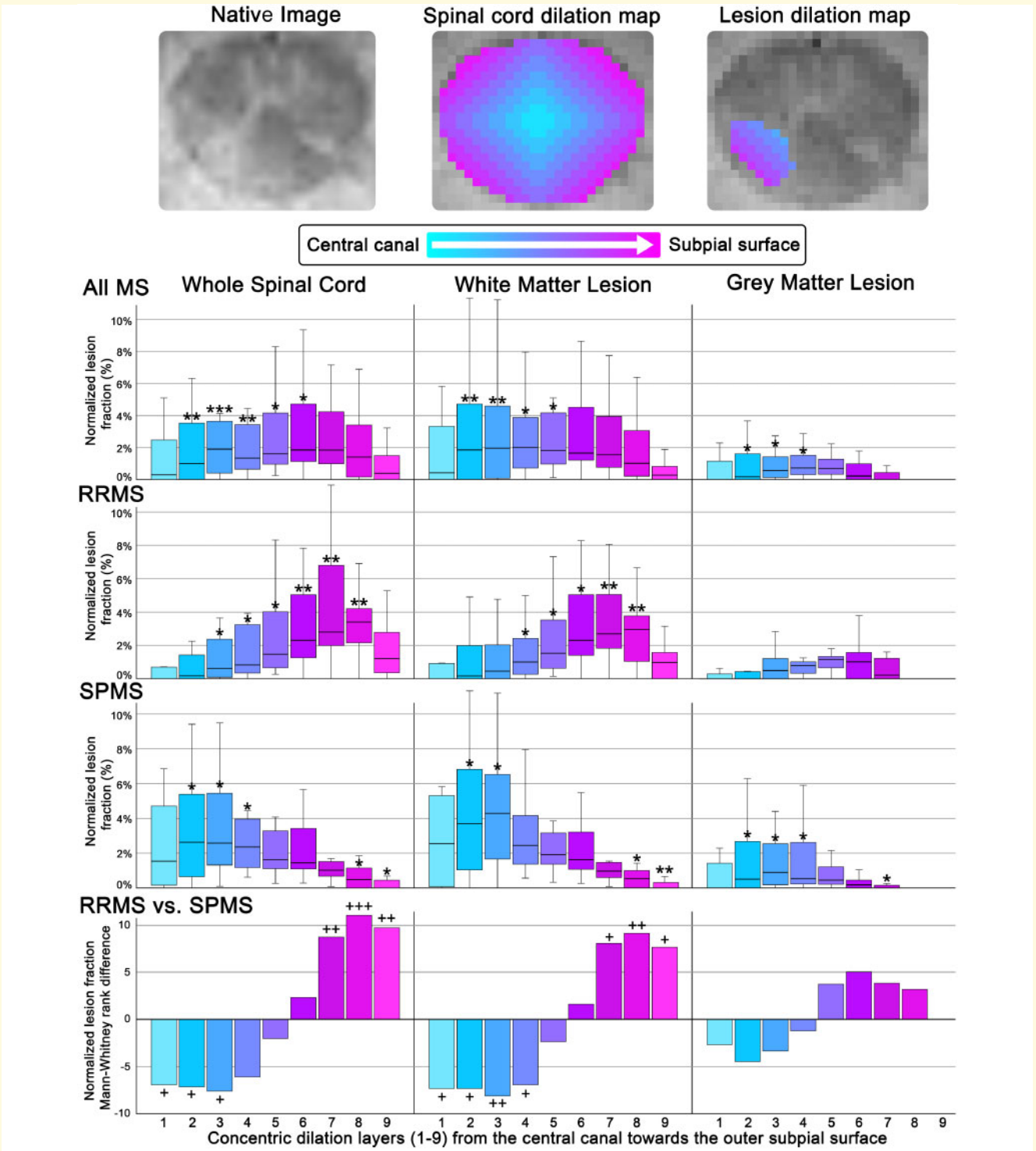

Figure 3 Spinal cord lesion mapping processing and results. Representative example of a native C1 lesion in an SPMS participant (female, 40 years old, disease duration: 6.7 years, EDSS: 3.5) alongside the corresponding concentric ring and concentric lesion map for the 9 layers. Box-and-whisker plots depict the lesioned fraction (*y*-axis) normalized to the respective radial dilation layer volume and individual multiple sclerosis (MS) participant total lesion volume. The concentric distance (*x*-axis) from the central canal CSF surface (layer 0, cyan) extending towards the outer subpial surface (layer 9, magenta) for the whole lesion, grey and white matter fractions in all multiple sclerosis, RRMS and SPMS participants, respectively. Error bars represent the 95% confidence interval for the respective lesioned tissue dilation level. Bar graphs depict the Mann-Whitney U-test rank difference between the RRMS and SPMS subtypes for the respective dilation layers. *P*-values reported are exploratory, and therefore not corrected for multiple comparisons. Exploratory comparison of individual-level lesion fraction compared to the median of the inner-most level (**P*-value < 0.05, ***P*-value < 0.01, ****P*-value < 0.001 by Wilcoxon signed-rank test, two-tailed, equal variances not assumed). Exploratory comparison of RRMS versus SPMS participants (^{+}P-value < 0.05, ^{++}P-value < 0.01, ^{+++}P-value < 0.001, by Mann-Whitney U-test (two-tailed, equal variances not assumed).

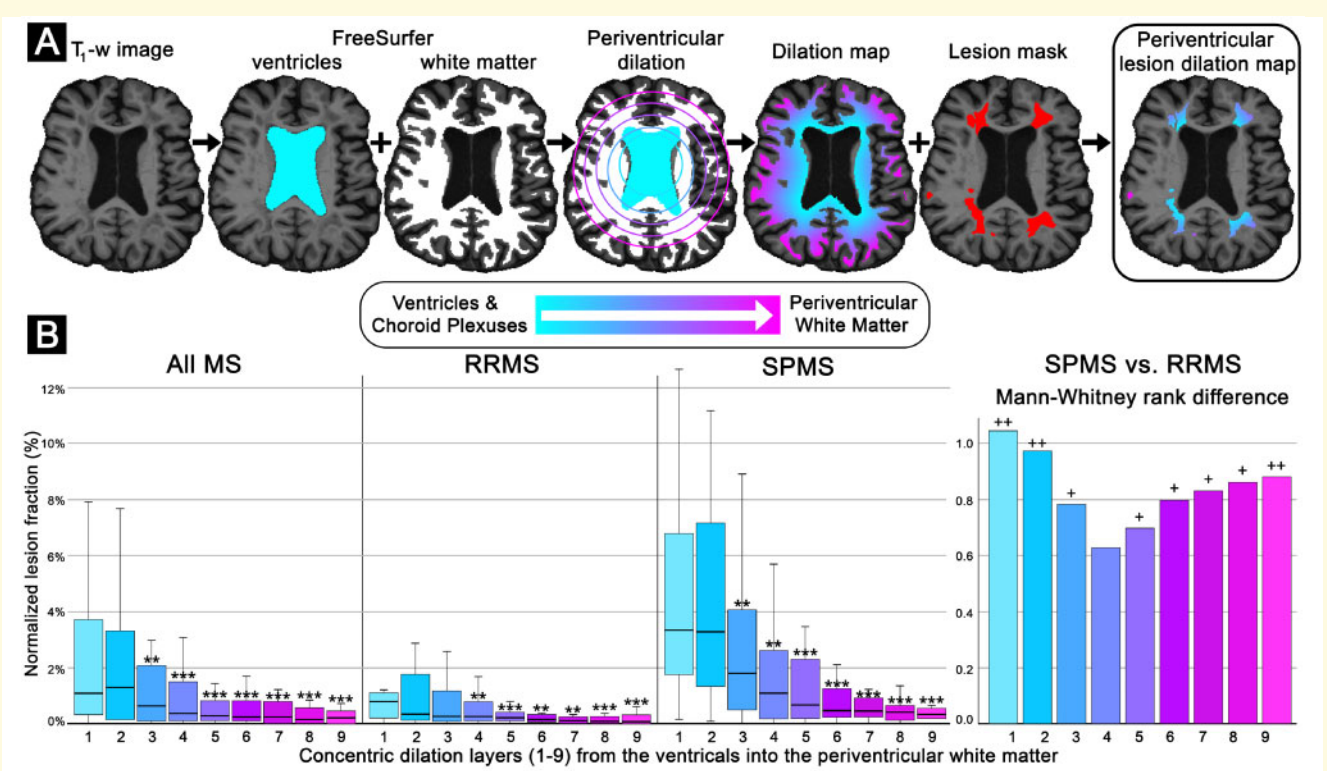

Figure 4 Brain lesion mapping processing pipeline and results. (**A**) Processing pipeline. Representative example of brain lesion mapping in an SPMS participant (female, 63 years old, disease duration: 33 years, EDSS: 2). The ventricle and choroid plexus segmentations from FreeSurfer were combined and used as a reference from which concentric 3D voxel-wise dilations expanded radially using scikit-image. The concentric dilation map was then masked using the lesion mask in FreeSurfer to isolate the lesion dilation map, which can then measure lesion fraction as a function of distance from the ventricular system CSF. (**B**) Brain lesion mapping results. Box-and-whisker plots depict the lesioned fraction (*y*-axis) normalized to the respective radial dilation layer volume and individual multiple sclerosis (MS) participant lesion volume. The concentric distance (*x*-axis) from the ventricular system (layer 0, cyan) extending inwards within the periventricular white matter (layer 9, magenta) in all multiple sclerosis, RRMS and SPMS participants, respectively. Error bars represent the 95% confidence interval for the respective lesioned tissue dilation level. Bar graphs depict the Mann-Whitney U-test rank difference between the SPMS and RRMS subtypes for the respective dilation layers. *P*-values reported are exploratory, and therefore not corrected for multiple comparisons. Exploratory comparison of individual-level lesion fraction compared to the median of the inner-most level (*P-value < 0.05, **P-value < 0.01, ***P-value < 0.001 by Wilcoxon signed-rank test, two-tailed, equal variances not assumed). Exploratory comparison of SPMS versus RRMS participants (^{+}P-value < 0.05, ^{++}P-value < 0.01, by Mann-Whitney U-test (two-tailed, equal variances not assumed).

lower mean spinal cord cross-sectional area relative to healthy control subjects, in both the grey matter ($P = 0.021$) and white matter ($P = 0.019$), but there were no significant differences between RRMS and SPMS groups. There was, however, a difference in the normalized proportion of spinal cord lesioned tissue in the grey and white matter, though this only reached significance in the white matter ($P = 0.05$). The spinal cord grey and white matter lesion fractions were found to be related ($\rho = 0.91$, $P < 0.001$). All of the multiple sclerosis participants with spinal cord lesions had portions within the grey and white matter, except for two multiple sclerosis participants (one SPMS and one RRMS) who only had white matter spinal cord lesions. Patients with multiple sclerosis had thinner cortices as compared to control subejcts ($P = 0.017$), with greater cortical thinning in SPMS than RRMS participants ($P < 0.001$). The spinal cord lesion fraction in the grey and white matter were found to be associated with white matter lesions in the brain ($r = 0.39$, $P = 0.021$ and $r = 0.37$, $P = 0.033$). The full exploratory bivariate correlation results of the brain and cervical spinal cord MRI metrics are shown in Supplementary Table 1.

Lesion mapping as a function of distance from CSF

The results of the cervical spinal cord lesion mapping are detailed below and further summarized in Fig. 3. Through inside-out assessment, spinal cord lesions were found to be dispersed in a pseudo-bell curve pattern, being partially skewed towards the two CSF surfaces bordering the spinal cord. When comparing the whole lesion fraction in RRMS and SPMS participants, we identified that the inner/outer bimodal skewness observed in the whole multiple sclerosis cohort was primarily driven by RRMS participants' greater

predominance for lesion formation in the outer subpial portion of the cervical cord and SPMS participants predominance for lesion formation in the inner portion of the cervical spinal cord nearer the central canal. The whole lesion fraction (%) was greater in RRMS participants relative to SPMS participants at layer 7 (2.8 ± 4.9% versus 1.0 ± 1.1%, $P = 0.005$), layer 8 (3.4 ± 2.2% versus 0.4 ± 1.1%, $P < 0.001$), layer 9 (1.2 ± 2.5% versus 0.0 ± 0.5%, $P = 0.002$) from the central canal CSF surface to the subpial CSF surface. In SPMS participants, compared to RRMS participants, lesions were predominantly located in the layers nearest the central canal CSF surface, within layer 1 (1.6 ± 5.1% versus 0.0 ± 1.1%, $P = 0.029$), layer 2 (2.6 ± 6.1% versus 0.2 ± 1.6%, $P = 0.023$), layer 3 (2.6 ± 5.5% versus 0.6 ± 2.4%, $P = 0.016$) and layer 4 (2.4 ± 3.4% versus 0.8 ± 2.9%, $P = 0.057$) from the central canal to the cord perimeter. These lesion distributions are retained when considering the lesion fractions within the grey and white matter tissues. When considering only the white matter spinal cord lesion component, the distribution pattern was very similar for all multiple sclerosis participants and disease subtypes. Subjects with RRMS were again found to have a higher predominance of white matter lesions in the outer layers, primarily at layer 7 (2.6 ± 3.5% versus 1.0 ± 0.9%, $P = 0.01$), layer 8 (2.8 ± 2.7% versus 0.5 ± 1.0%, $P = 0.003$), and layer 9 (0.9 ± 1.6% versus 0.2 ± 0.3%, $P = 0.016$) outer portion of the cervical spinal cord. In contrast, SPMS participants showed, relative to RRMS subjects, a higher inner predominance for white matter pathology in layer 1 (2.5 ± 5.4% versus 0.0 ± 1.3%, $P = 0.02$), layer 2 (3.7 ± 6.7% versus 1.5 ± 2.2%, $P = 0.02$), layer 3 (4.3 ± 5.6% versus 0.5 ± 2.3%, $P = 0.009$) and layer 4 (2.4 ± 3.4% versus 1.0 ± 2.2%, $P = 0.029$). The grey matter lesion distribution followed a similar pattern, however, shifted more internally with a narrower distribution across fewer levels. Additionally, to confirm our findings, we performed further analyses mapping the spinal cord lesion distribution by eroding from the outer subpial portion of the spinal cord towards the central canal. The results of these analyses were largely overlapping and presented with a similar overall pattern as compared to the inside-out mapping (central canal towards subpial) and can be found in the Supplementary material.

The results of the brain periventricular lesion mapping are detailed below and further summarized in Fig. 4. Through inside-out assessment white matter multiple sclerosis lesions in the brain were found to preferentially occur with nearer proximity to the ventricular system. The gradient pattern of lesions originating nearer the CSF, while present in both disease stages, was particularly evident in SPMS cases. Additionally, the normalized lesion fraction (%) was greater in participants diagnosed with SPMS as compared to RRMS across most all the periventricular layers. The largest difference between SPMS and RRMS subtypes was identified in the two layers nearest the CSF, layer 1 (3.3 ± 6.2% versus 0.8 ± 1.1%, $P = 0.002$) and layer 2 (3.3 ± 6.5% versus 0.3 ± 1.8%, $P = 0.004$), respectively.

Clinical correlations with spinal cord and brain MRI metrics

The statistically significant associations between the MRI and clinical metrics (Supplementary Table 2) at bivariate analysis were used as input for the linear regression analysis for each of the respective clinical metrics. Stepwise linear regression results and the respective correlation plots are further depicted in Fig. 5. Stepwise linear regression identified cortical thickness as the most significant ($\beta = -0.55$, $R^2 = 0.30$, $P = 0.002$) contributor to EDSS. Stepwise linear regression identified a combined model ($R^2 = 0.44$) of white matter lesion fraction in the spinal cord ($\beta = 0.44$, $P = 0.01$) and brain ($\beta = 0.40$, $P = 0.02$) as the most significant contributors to fine motor skill disability measured through the 9-HPT. Reduced walking speed, measured by the Timed 25-Foot Walk test, was found to be best explained through a stepwise linear regression model that combined ($R^2 = 0.32$) cortical thickness ($\beta = -0.48$, $P = 0.008$) and spinal cord grey matter cross-sectional area ($\beta = -0.37$, $P = 0.035$).

Discussion

In this study, we used ultra-high field strength 7 T MRI to characterize the distribution of grey and white matter lesions in the cervical spinal cord and brain of a heterogeneous multiple sclerosis cohort. Lesions throughout the CNS were mapped on the basis of their proximity to the CSF brain and spinal cord surfaces to determine the presence of an outside-in pathological gradient throughout the CNS. We also assessed the relationship between spinal and brain pathology and their relative contributions to measures of neurological disability. We found that spinal cord lesions have a greater propensity to manifest nearer the central canal and subpial CSF interfaces. Similarly, white matter brain lesions were found to originate nearest to the CSF in the ventricular system. Interestingly, both patterns of cervical spinal cord and brain lesion distribution varied between multiple sclerosis subtypes. In the brain, the distribution varied in the degree of the periventricular pathological gradient between RRMS and SPMS. However, in the cervical spinal cord, the pathological gradient differed in the CSF surface from which the gradient originated, with the subpial surface being implicated in early RRMS and then shifted towards the central canal in the latter SPMS stage of the disease. Both spinal cord and brain MRI metrics were found to contribute to neurological disability.

Spinal cord pathology at 7 T

Spinal cord lesions were identified in 83% of participants diagnosed with multiple sclerosis, a comparable rate to that of a previous report that found an increase of spinal cord lesion detection with 7 T relative to 3 T MRI (Dula *et al.*, 2016). All SPMS participants had spinal cord lesions compared to five of the RRMS participants that did not.

Table 2 MRI results for the spinal cord and brain

	Controls	All MS	RRMS	SPMS
Spinal cord MRI metrics				
Presence of spinal cord lesions, *n*, yes/no	0/11	29/6	14/6	15/0
Cross-sectional area, mm^2				
Grey matter	7.70 ± 0.94 **$P = 0.021$**[a]	6.8 ± 1.5	7.2 ± 1.5	6.2 ± 1.5
White matter	58.1 ± 4.9 **$P = 0.019$**[a]	52.8 ± 9.2	55.2 ± 9.5	49.6 ± 8.1
Lesion fraction, %				
Grey matter	–	6.8 ± 18.1	2.0 ± 2.9	13.2 ± 26.5
White matter	-	5.5 ± 9.4	2.6 ± 2.9 **$P = 0.050$**[c]	9.3 ± 13.3
Lesion volume, mm^3				
Grey matter	–	19.6, 47.1	19.9, 33.9	19.6, 97.8
White matter	–	193, 248	212, 268	192, 278
Brain MRI metrics				
Cortical thickness, mm	2.41 ± 0.07 **$P = 0.017$**[a]	2.33 ± 0.12	2.40 ± 0.10 **$P < 0.001$**[b]	2.26 ± 0.10
Cortical lesion volume, mm^3	-	201, 625	143, 439 **$P = 0.035$**[c]	331, 779
Fraction, %	-	0.013, 0.041	0.009, 0.031 **$P = 0.035$**[c]	0.025, 0.071
White matter lesion Volume, mm^3	-	1454, 4668	903, 3037 **$P = 0.004$**[c]	5554, 15600
Fraction, %	-	0.11, 0.31	0.062, 0.21 **$P = 0.004$**[c]	0.33, 1.1

All values are reported as mean ± standard deviation for normally distributed variables or median, interquartile range for non-normally distributed variables. All spinal cord lesion fractions are provided as the mean proportion of lesion tissue normalized by the respective tissue volume and the cortical and white matter lesion volumes are normalized by the intracranial volume.

[a]*P*-value, healthy controls versus all multiple sclerosis participants by unpaired two-tailed *t*-test (equal variances not assumed).

[b]*P*-value, RRMS versus SPMS participants by unpaired two-tailed *t*-test (equal variances not assumed).

[c]*P*-value, RRMS versus SPMS participants by Mann-Whitney U-test (two-tailed).

Overall, those with multiple sclerosis had evidence of grey and white matter spinal cord atrophy with significantly lower grey and white matter cervical spinal cord cross-sectional area relative to control subjects. Two previous *in vivo* spinal cord studies in multiple sclerosis have reported an increased propensity for lesion development in the grey matter of participants with a more progressive disease course (Kearney *et al.*, 2015*b*; Eden *et al.*, 2019). In this cohort, we found no significant difference in the normalized proportion of global lesioned tissue in the grey matter between subtypes, though progressive multiple sclerosis cases exhibited an overall larger fraction of lesion tissue.

Lesion proximity to the CSF

To understand the distribution of cervical spinal cord pathology in our multiple sclerosis participant cohort, we mapped lesioned tissue as a function of distance from the inner CSF central canal surface, projecting through the central spinal cord tissue and extending to the outer subpial CSF surface. We found that subjects with multiple sclerosis had a greater propensity to manifest spinal cord lesions nearer the central canal and the subpial CSF interfaces. Subjects with RRMS and SPMS also exhibited a strong gradient of brain white matter lesions nearest the ventricular system, and this pattern was particularly evident in SPMS.

Our findings echo those from previous brain histopathological studies, which suggested that meningeal inflammation via CSF soluble pro-inflammatory mediators may be linked to pathogenic lesion development in the brain (Frischer *et al.*, 2009; Lucchinetti *et al.*, 2011; Zurawski *et al.*, 2017) and spinal cord (Androdias *et al.*, 2010), thereby proposing the presence of an outside-in neuropathological gradient in multiple sclerosis (Magliozzi *et al.*, 2010). An early histopathological description of spinal cord lesion morphology characterized plaques to be triangular, with the base along the outer subpial surface and the tip penetrating inwards towards the central canal (Fog, 1950). *In vivo* brain neuroimaging studies have similarly identified an outside-in neuropathological gradient extending from the juxtameningeal border into the cortical grey matter (Mainero *et al.*, 2015), a CSF outside-in gradient of thalamic damage in adult multiple sclerosis (Louapre *et al.*, 2018) and paediatric multiple sclerosis (Fadda *et al.*, 2019), as well as from the CSF periventricular border into the surrounding white matter (Liu *et al.*, 2015; Brown *et al.*, 2017, 2020). A gradient of spinal cord subpial magnetization transfer ratio abnormalities has also been identified in multiple sclerosis, using

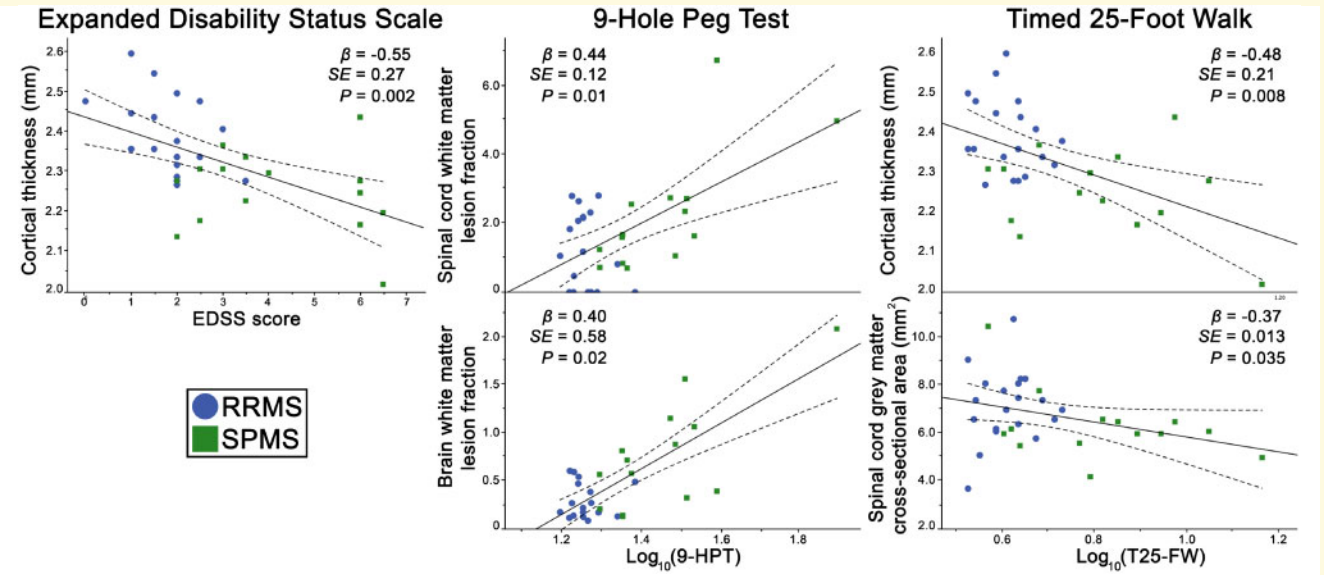

Figure 5 Associations of MRI metrics with clinical disability measures. Correlation plots between the clinical disability measures and the most significant MRI metric contributor (identified through stepwise linear regression), linearly illustrated with regression lines (dotted lines representing 95% confidence intervals). T25-FW = Timed 25-Foot Walk.

microstructural MRI at 3 T, in association with multiple sclerosis disability measures (Kearney *et al.*, 2014). A large study composed of >1000 participants identified increased lesion frequency in areas bordering the ventricular system (Holland *et al.*, 2012).

In this study, we found that participants with early RRMS had a greater proportion of spinal cord lesioned tissue nearer the outer meningeal subpial surface, suggesting that the CSF may play an important role in lesion development in the early stage of the disease. Meningeal inflammation along the outer subpial CSF surface has also been histopathologically identified in clinically isolated syndrome and RRMS cases (Frischer *et al.*, 2009; Lucchinetti *et al.*, 2011). Inversely, we found that subjects with SPMS had a greater amount of lesioned tissue nearest the central canal along the inner portion of the spinal cord. A large study of 642 multiple sclerosis participants found that not only do spinal cord lesion locations differ between RRMS and SPMS subtypes, but that the location is also linked to clinical disability (Eden *et al.*, 2019). In the brain, we identified a strong gradient of lesioned tissue nearest the ventricular system, in particular for those with SPMS. Previous studies in the brain have similarly found an increase of lesion (Holland *et al.*, 2012) and magnetization transfer abnormalities (Liu *et al.*, 2015; Brown *et al.*, 2020) in those with SPMS occurring in the periventricular area, but also within the cortex, where lesion accrual was also found to greater for those with SPMS than RRMS (Treaba *et al.*, 2019). Overall our findings suggest that the dynamics of the CSF outside-in penetrating factors may potentially differ between the two multiple sclerosis subtypes. The observed shift in lesion localization between the two multiple sclerosis subtypes could be attributed to different factors contributing to lesion retraction, including repair mechanisms, resolution of microstructural oedema and development of atrophy within lesions (Dwyer *et al.* 2018). It is also possible that the inner and outer CSF surfaces potentially manifest different susceptibility to these pathological components.

The exact mechanisms underlying the pathogenesis and dynamics of the putative CSF inflammatory mediators are not yet well understood (Magliozzi *et al.*, 2010; Fischer *et al.*, 2013; Trapp *et al.*, 2018). Some CSF soluble candidates, including ceramide (Vidaurre *et al.*, 2014) and semaphorin (Chiou *et al.*, 2018) have been proposed. It is theorized that these factors may enter the CSF through the choroid plexus into the ventricular system (Vercellino *et al.*, 2008) and also through inflamed meninges bordering the brain and spinal cord (Magliozzi *et al.*, 2010; Androdias *et al.*, 2010). In our study, the pattern of spinal cord lesion distribution observed in RRMS and SPMS subjects originated from these two CSF surfaces. In a model of experimental autoimmune encephalitis, the choroid plexus was demonstrated as a point of lymphocyte penetrance into the CNS that preceded lymphocyte entry via the blood–brain barrier (Reboldi *et al.*, 2009). Additionally, in a mouse model, healing macrophages were found to traverse the choroid plexus entering the CSF and routed through the ventricular system to the central canal in response to spinal cord injury (Shechter *et al.*, 2013). Immune activation of the choroid plexus has also been identified to associate with HLA-DR (Vercellino *et al.*, 2008), one of the strongest genetic susceptibility loci in multiple sclerosis (*HLA-DRB1*), which has also been suggested to influence spinal cord pathology (DeLuca *et al.*, 2013). *In vivo* imaging of intrathecally

administered contrast agent in humans spread first from the subpial surface to neighbouring deeper brain areas (Ringstad *et al.*, 2017) and was also found to begin in the periventricular white matter (Ringstad *et al.*, 2018), which verified a similar pattern of CSF influx into the parenchyma observed in mice (Iliff *et al.*, 2012). Therefore, CSF-borne neurotoxic factors may enter the parenchyma via the Virchow-Robin perivascular spaces along blood vessels branching into the inner ependymal central canal/ventricle surface or the outer meningeal/subpial surface (Millen and Woollam, 1961; Esiri and Gay, 1990; Iliff *et al.*, 2012; Lassmann, 2018). Once within the parenchymal interstitium, cytotoxic factors may follow the bulk flow of the interstitial fluid towards the perivenular space to then provoke lesion development around venules possibly involving an associated lymphatic vessel (Oppenheimer, 1978; Rasmussen, *et al.*, 2018).

Associations of *in vivo* spinal cord and brain pathology

We found few significant associations between the brain and spinal cord MRI metrics related to lesion fractions in the spinal cord grey/white matter in associations with brain white matter lesions. Our findings are in agreement with a previous 3 T MRI study that reported a weak relationship between the brain and spinal cord involvement, with regard to both lesions and atrophy (Cohen *et al.*, 2012).

Clinical relevance

Clinical neurological disability was assessed using three of the most commonly acquired physical disability metrics, EDSS, 9-HPT, and Timed 25-Foot Walk. As expected, RRMS and SPMS subtypes had clinically distinct disability profiles and were found to be influenced by a combination of the spinal cord and brain MRI metrics. The only spinal cord MRI metrics that were found to differ between the two subtypes was the inside versus outside spinal cord lesion pathological distribution profiles and the normalized white matter lesion fraction. Stepwise linear regression identified cortical thickness as having the most appreciable relationship to the EDSS score. EDSS, despite being heavily weighted towards motor disability, reflects a spectrum of symptomatology, including motor, sensory, sphincter, visual, and cognitive dysfunction. Similarly, a longitudinal study found cortical lesion volume to be predictive of subsequent disease disability progression over time by EDSS (Treaba *et al.*, 2019). We found that fine motor disability was primarily associated with lesioned tissues bordering the ventricular system and central, with brain and spinal cord white matter lesion fractions having the greatest contribution to the 9-HPT score. Inversely, walking difficulty was associated with atrophy in the grey matter of the spinal cord and brain that borders the meninges, with cortical thickness and spinal cord grey matter cross-sectional area found to account for the most variance seen in Timed 25-Foot Walk scores. These spatially specific and clinically distinct correlational findings with disability metrics are supportive of a coupled underlying pathological process present within the brain and spinal cord that seems to be dynamic between multiple sclerosis subtypes.

Limitations and future directions

Six participants were excluded from cortical lesion segmentation due to movement artefacts, which limited the characterization of the relationship between cortical and spinal cord lesions, as previous studies have reported strong significant relationships between cortical lesions and disability (Nielsen *et al.*, 2013; Mainero *et al.*, 2015). Those six participants' lesion masks were generated using the 3 T scans instead of the 7 T images. Previous findings, however, have demonstrated that white matter lesion volume assessment does not significantly differ between the two field strengths (De Graaf *et al.*, 2013). As cervical spinal cord MRI metrics could reflect, at least in part, pathology in the more distal aspects of the spinal cord (Kearney *et al.*, 2015*a*), future investigations should include the thoracic and lumbar segments, though this remains technically challenging at 7 T (Schlaeger *et al.*, 2014). All multiple sclerosis participants included in the study were diagnosed in accordance with the concurrent (2010) McDonald diagnostic criteria (Polman *et al.*, 2011). The SPMS cohort included some SPMS participants who had recently converted from RRMS to SPMS. Therefore, some of the SPMS participants may be considered early stage with relatively low EDSS scores. However, it must also be noted that while EDSS does incorporate an aspect of cognitive disability, it is strongly weighted towards motor disability, therefore underestimating disability related to other clinical components.

While ultra-high field strength data remain limited, particularly for the spinal cord, these results show that cervical 7 T MRI can be applied in a clinically acceptable time frame (MAGNIMS study group, 2015), <5 min, and provide useful information of an individual's current multiple sclerosis disease status. Particularly now that 7 T MRI has been approved for clinical MRI applications (Sati, 2018). Importantly, combining neuroimaging with CSF-borne cellular biomarkers to link the observed neuroimaging and molecular medicine definitions of disease activity would prove valuable in characterizing the pathophysiological processes driving the chronic inflammation seen in multiple sclerosis. Incorporation of CSF sampling in neuroimaging studies may prove highly valuable to analyse markers for neural damage by glial activation (GFAP and YKL), astrocyte activation (chitinase), macrophage activation (CD163) (Stilund *et al.*, 2014; Lassmann, 2019; Magliozzi *et al.*, 2019), or active intrathecal inflammation (Bielekova *et al.*, 2012). The combination of CSF-borne protein profiling with machine learning (Barbour *et al.*, 2017) and metabolomic profiling (Stoessel *et al.*, 2018) with neuroimaging end points, may shed light on the pathological processes driving the differences observed between multiple sclerosis subtypes (Lassmann, 2019). Importantly, very interesting findings have implicated

the role of the gut microbiota in humans and mice in modulating T cell activity (Berer *et al.*, 2017; Cekanaviciute *et al.*, 2017; Kadowaki *et al.*, 2019).

Conclusions

In summary, we used 7 T MRI to characterize lesion distribution in the cervical spinal cord in subjects with multiple sclerosis by mapping lesions as a function of distance from the CSF surface. We identified a pathological profile of spinal cord lesion distribution with a strong relation to the CSF proximity that demonstrates distinct patterns according to multiple sclerosis subtypes. A pattern of lesion distribution based on proximity to the CSF was also observed in the periventricular region of the brain. Overall, these findings are in support of the outside-in theory of CSF-/ependymal-mediated inflammatory pathogenesis for multiple sclerosis demyelination, whereby CSF-borne immune cytotoxic factors penetrate the parenchyma to provoke focal lesion formation/expansion and produce a gradient of diffuse demyelination.

Acknowledgements

We would like to thank the participants for their commitment and continued efforts in supporting our research.

Funding

This study was supported by a grant of the National Institute of Health (NIH R01NS07832201 A1) as well as by EMD Serono. R.O. was supported by MultipleMS (EU Horizon 2020 grant 733161) and COMBAT-MS (Patient-Centered Outcomes Research Institute grant MS-1511–33196). T.G. was supported by Stockholm City Council and Karolinska Institutet (ALF grants 20120213 and 20150166) and the Swedish Society for Medical Research (post-doctoral fellowship). E.H. was supported by the National Multiple Sclerosis Society (fellowship FG-1507-05459). Funded by the Canada Research Chair in Quantitative Magnetic Resonance Imaging (950-230815), the Canadian Institute of Health Research (CIHR FDN-143263), the Canada Foundation for Innovation [32454, 34824], the Fonds de Recherche du Québec—Santé (28826), the Fonds de Recherche du Québec—Nature et Technologies (2015-PR-182754), the Natural Sciences and Engineering Research Council of Canada [435897-2013], the Canada First Research Excellence Fund (IVADO and TransMedTech) and the Quebec BioImaging Network (5886).

Competing interests

E.C.K. has received research grants from Atlas5D, Biogen, EMD Serono and Roche; and consulting fees from Acorda, Atlas5D, Biogen, EMD Merck Serono, Genentech and Shire. R.B. has received consulting fees from EMD Serono, Genentech, Sanofi Genzyme, and Novartis and research support from Biogen, EMD Merck Serono, Novartis, and Sanofi Genzyme. C.M. has received research support from EMD Merck Serono and Sanofi Genzyme, as well as speaker fees from Biogen. All other authors report no competing interests.

Supplementary material

Supplementary material is available at *Brain* online.

References

Adams CWM, Abdulla YH, Torres EM, Poston RN. Periventricular lesions in multiple sclerosis: their perivenous origin and relationship to granular ependymitis. Neuropathol Appl Neurobiol 1987; 13: 141–52.

Agosta F, Pagani E, Caputo D, Filippi M. Associations between cervical cord gray matter damage and disability in patients with multiple sclerosis. Arch Neurol 2007; 64: 1302.

Androdias G, Reynolds R, Chanal M, Ritleng C, Confavreux C, Nataf S. Meningeal T cells associate with diffuse axonal loss in multiple sclerosis spinal cords. Ann Neurol 2010; 68: 465–76.

Barbour C, Kosa P, Komori M, Tanigawa M, Masvekar R, Wu T, et al. Molecular-based diagnosis of multiple sclerosis and its progressive stage. Ann Neurol 2017; 82: 795–812.

Barry RL, Vannesjo SJ, By S, Gore JC, Smith SA. Spinal cord MRI at 7T. Neuroimage 2018; 168: 437–51.

Berer K, Gerdes LA, Cekanaviciute E, Jia X, Xiao L, Xia Z, et al. Gut microbiota from multiple sclerosis patients enables spontaneous autoimmune encephalomyelitis in mice. Proc Natl Acad Sci USA 2017; 114: 10719–24.

Bielekova B, Komori M, Xu Q, Reich DS, Wu T. Cerebrospinal fluid IL-12p40, CXCL13 and IL-8 as a combinatorial biomarker of active intrathecal inflammation. PLoS One 2012; 7: e48370.

Benjamini Y, Hochberg Y. Controlling the false discovery rate: a practical and powerful approach to multiple testing. J R Stat Soc Ser B Methodol 1995; 57: 289–300.

Brown JWL, Chowdhury A, Kanber B, Prados Carrasco F, Eshaghi A, Sudre CH, et al. Magnetisation transfer ratio abnormalities in primary and secondary progressive multiple sclerosis. Mult Scler 2020; 26: 679–87.

Brown JWL, Pardini M, Brownlee WJ, Fernando K, Samson RS, Prados Carrasco F, et al. An abnormal periventricular magnetization transfer ratio gradient occurs early in multiple sclerosis. Brain 2017; 140: 387–98.

Cekanaviciute E, Yoo BB, Runia TF, Debelius JW, Singh S, Nelson CA, et al. Gut bacteria from multiple sclerosis patients modulate human T cells and exacerbate symptoms in mouse models. Proc Natl Acad Sci USA 2017; 114: 10713–8.

Chiou B, Lucassen E, Sather M, Kallianpur A, Connor J. Semaphorin 4A and H-Ferritin utilize Tim-1 on human oligodendrocytes: a novel neuro-immune axis. Glia 2018; 66: 1317–30.

Cohen AB, Neema M, Arora A, Dell'Oglio E, Benedict RHB, Tauhid S, et al. The relationships among MRI-defined spinal cord involvement, brain involvement, and disability in multiple sclerosis. J Neuroimaging 2012; 22: 122–8.

Dawson J. The histology of disseminated sclerosis. Lancet 1916; 187: 1090–1.

De Graaf WL, Kilsdonk ID, Lopez-Soriano A, Zwanenburg JJM, Visser F, Polman CH, et al. Clinical application of multi-contrast 7-

T MR imaging in multiple sclerosis: increased lesion detection compared to 3 T confined to grey matter. Eur Radiol 2013; 23: 528–40.
De Leener B, Fonov VS, Collins DL, Callot V, Stikov N, Cohen-Adad J. PAM50: unbiased multimodal template of the brainstem and spinal cord aligned with the ICBM152 space. Neuroimage 2018; 165: 170–9.
De Leener B, Kadoury S, Cohen-Adad J. Robust, accurate and fast automatic segmentation of the spinal cord. Neuroimage 2014; 98: 528–36.
De Leener B, Lévy S, Dupont SM, Fonov VS, Stikov N, Louis Collins D, et al. SCT: Spinal Cord Toolbox, an open-source software for processing spinal cord MRI data. Neuroimage 2017; 145: 24–43.
DeLuca GC, Alterman R, Martin JL, Mittal A, Blundell S, Bird S, et al. Casting light on multiple sclerosis heterogeneity: the role of HLA-DRB1 on spinal cord pathology. Brain 2013; 136: 1025–34.
Dula AN, Pawate S, Dortch RD, Barry RL, George-Durrett KM, Lyttle BD, et al. Magnetic resonance imaging of the cervical spinal cord in multiple sclerosis at 7T. Mult Scler J 2016; 22: 320–8.
Dupont SM, De Leener B, Taso M, Le Troter A, Nadeau S, Stikov N, et al. Fully-integrated framework for the segmentation and registration of the spinal cord white and gray matter. Neuroimage 2017; 150: 358–72.
Dwyer MG, Bergsland N, Ramasamy DP, Jakimovski D, Weinstock-Guttman B, Zivadinov R. Atrophied brain lesion volume: a new imaging biomarker in multiple sclerosis. J Neuroimaging 2018; 28: 490–5.
Eden D, Gros C, Badji A, Dupont SM, De Leener B, Maranzano J, et al. Spatial distribution of multiple sclerosis lesions in the cervical spinal cord. Brain 2019; 142: 633–46.
Esiri MM, Gay D. Immunological and neuropathological significance of the Virchow-Robin space. J Neurol Sci 1990; 100: 3–8.
Fadda G, Brown RA, Magliozzi R, Aubert-Broche B, O'Mahony J, Shinohara RT, et al. A surface-in gradient of thalamic damage evolves in pediatric multiple sclerosis. Ann Neurol 2019; 85: 340–51.
Fedorov A, Beichel R, Kalpathy-Cramer J, Finet J, Fillion-Robin J-C, Pujol S, et al. 3D Slicer as an image computing platform for the Quantitative Imaging Network. Magn Reson Imaging 2012; 30: 1323–41.
Fischer MT, Wimmer I, Höftberger R, Gerlach S, Haider L, Zrzavy T, et al. Disease-specific molecular events in cortical multiple sclerosis lesions. Brain 2013; 136: 1799–815.
Fischl B. FreeSurfer. Neuroimage 2012; 62: 774–81.
Fog T. Topographic distribution of plaques in the spinal cord in multiple sclerosis. Arch Neurol Psychiatry 1950; 63: 382–414.
Fog T. The topography of plaques in multiple sclerosis with special reference to cerebral plaques. Acta Neurol Scand, Suppl 1965; 15: 1–161.
Frischer JM, Bramow S, Dal-Bianco A, Lucchinetti CF, Rauschka H, Schmidbauer M, et al. The relation between inflammation and neurodegeneration in multiple sclerosis brains. Brain 2009; 132: 1175–89.
Gass A, Rocca MA, Agosta F, Ciccarelli O, Chard D, Valsasina P, et al. MRI monitoring of pathological changes in the spinal cord in patients with multiple sclerosis. Lancet Neurol 2015; 14: 443–54.
Gilmore CP, Bo L, Owens T, Lowe J, Esiri MM, Evangelou N. Spinal cord gray matter demyelination in multiple sclerosis—a novel pattern of residual plaque morphology. Brain Pathol 2006; 16: 202–8.
Gilmore CP, DeLuca GC, Bö L, Owens T, Lowe J, Esiri MM, et al. Spinal cord neuronal pathology in multiple sclerosis. Brain Pathol 2009; 19: 642–9.
Greve DN, Fischl B. Accurate and robust brain image alignment using boundary-based registration. Neuroimage 2009; 48: 63–72.
Gros C, De Leener B, Dupont SM, Martin AR, Fehlings MG, Bakshi R, et al. Automatic spinal cord localization, robust to MRI contrasts using global curve optimization. Med Image Anal 2018; 44: 215–27.
Holland CM, Charil A, Csapo I, Liptak Z, Ichise M, Khoury SJ, et al. The relationship between normal cerebral perfusion patterns and white matter lesion distribution in 1,249 patients with multiple sclerosis. J Neuroimaging 2012; 22: 129–36.
Iliff JJ, Wang M, Liao Y, Plogg BA, Peng W, Gundersen GA, et al. A paravascular pathway facilitates CSF flow through the brain parenchyma and the clearance of interstitial solutes, including amyloid β. Sci Transl Med 2012; 4: 147ra111.
Jenkinson M, Beckmann CF, Behrens TEJ, Woolrich MW, Smith SM. FSL. Neuroimage 2012; 62: 782–90.
Kadowaki A, Saga R, Lin Y, Sato W, Yamamura T. Gut microbiota-dependent CCR9 + CD4 + T cells are altered in secondary progressive multiple sclerosis. Brain 2019; 142: 916–31.
Kearney H, Miller DH, Ciccarelli O. Spinal cord MRI in multiple sclerosis—diagnostic, prognostic and clinical value. Nat Rev Neurol 2015; 11: 327–38.
Kearney H, Schneider T, Yiannakas MC, Altmann DR, Wheeler-Kingshott C, Ciccarelli O, et al. Spinal cord grey matter abnormalities are associated with secondary progression and physical disability in multiple sclerosis. J Neurol Neurosurg Psychiatry 2015; 86: 608–14.
Kearney H, Yiannakas MC, Samson RS, Wheeler-Kingshott C, Ciccarelli O, Miller DH. Investigation of magnetization transfer ratio-derived pial and subpial abnormalities in the multiple sclerosis spinal cord. Brain 2014; 137: 2456–68.
Kilsdonk ID, Jonkman LE, Klaver R, van Veluw SJ, Zwanenburg JJM, Kuijer JPA, et al. Increased cortical grey matter lesion detection in multiple sclerosis with 7 T MRI: a post-mortem verification study. Brain 2016; 139: 1472–81.
Kurtzke JF. Rating neurologic impairment in multiple sclerosis: an expanded disability status scale (EDSS). Neurology 1983; 33: 1444.
Kutzelnigg A, Lassmann H. Cortical demyelination in multiple sclerosis: a substrate for cognitive deficits? J Neurol Sci 2006; 245: 123–6.
Lassmann H. Multiple sclerosis pathology. Cold Spring Harb Perspect Med 2018; 8: 3.
Lassmann H. Pathogenic mechanisms associated with different clinical courses of multiple sclerosis. Front Immunol 2019; 9: 3116.
Liu Z, Pardini M, Yaldizli Ö, Sethi V, Muhlert N, Wheeler-Kingshott CAM, et al. Magnetization transfer ratio measures in normal-appearing white matter show periventricular gradient abnormalities in multiple sclerosis. Brain 2015; 138: 1239–46.
Louapre C, Govindarajan ST, Giannì C, Madigan N, Sloane JA, Treaba CA, et al. Heterogeneous pathological processes account for thalamic degeneration in multiple sclerosis: insights from 7 T imaging. Mult Scler J 2018; 24: 1433–44.
Lucchinetti CF, Popescu BFG, Bunyan RF, Moll NM, Roemer SF, Lassmann H, et al. Inflammatory cortical demyelination in early multiple sclerosis. N Engl J Med 2011; 365: 2188–97.
Lumsden CE, Vinken PJ, Bruyn GW. The pathology of multiple sclerosis. Handbook Clin Neurol 1970; 9: 217–309.
Magliozzi R, Howell OW, Durrenberger P, Aricò E, James R, Cruciani C, et al. Meningeal inflammation changes the balance of TNF signalling in cortical grey matter in multiple sclerosis. J Neuroinflammation 2019; 16: 259.
Magliozzi R, Howell OW, Reeves C, Roncaroli F, Nicholas R, Serafini B, et al. A gradient of neuronal loss and meningeal inflammation in multiple sclerosis. Ann Neurol 2010; 68: 477–93.
Mainero C, Benner T, Radding A, van der Kouwe A, Jensen R, Rosen BR, et al. In vivo imaging of cortical pathology in multiple sclerosis using ultra-high field MRI. Neurology 2009; 73: 941–8.
Mainero C, Louapre C, Govindarajan ST, Giannì C, Nielsen AS, Cohen-Adad J, et al. A gradient in cortical pathology in multiple sclerosis by in vivo quantitative 7 T imaging. Brain 2015; 138: 932–45.
Millen JW, Woollam D. On the nature of the pia matter. Brain 1961; 84: 514–20.

Muccilli A, Seyman E, Oh J. Spinal cord MRI in multiple sclerosis. Neurol Clin 2018; 36: 35–57.

Nielsen AS, Kinkel RP, Madigan N, Tinelli E, Benner T, Mainero C. Contribution of cortical lesion subtypes at 7T MRI to physical and cognitive performance in MS. Neurology 2013; 81: 641–9.

MAGNIMS study group. MAGNIMS consensus guidelines on the use of MRI in multiple sclerosis—establishing disease prognosis and monitoring patients: evidence-based guidelines. Nat Rev Neurol 2015; 11: 597–606.

Oppenheimer DR. The cervical cord in mulitple sclerosis. Neuropathol Appl Neurobiol 1978; 4: 151–62.

Polman CH, Reingold SC, Banwell B, Clanet M, Cohen JA, Filippi M, et al. Diagnostic criteria for multiple sclerosis: 2010 Revisions to the McDonald criteria. Ann Neurol 2011; 69: 292–302.

Rasmussen MK, Mestre H, Nedergaard M. The glymphatic pathway in neurological disorders. Lancet Neurol 2018; 17: 1016–24.

Reboldi A, Coisne C, Baumjohann D, Benvenuto F, Bottinelli D, Lira S, et al. C-C chemokine receptor 6-regulated entry of TH-17 cells into the CNS through the choroid plexus is required for the initiation of EAE. Nat Immunol 2009; 10: 514–23.

Ringstad G, Valnes LM, Dale AM, Pripp AH, Vatnehol S-AS, Emblem KE, et al. Brain wide glymphatic enhancement and clearance in humans assessed with MRI. JCI Insight 2018; 3: 13.

Ringstad G, Vatnehol SAS, Eide PK. Glymphatic MRI in idiopathic normal pressure hydrocephalus. Brain 2017; 140: 2691–705.

Sati P. Diagnosis of multiple sclerosis through the lens of ultra-high-field MRI. J Magn Reson 2018; 291: 101–9.

Schlaeger R, Papinutto N, Panara V, Bevan C, Lobach IV, Bucci M, et al. Spinal cord gray matter atrophy correlates with multiple sclerosis disability: GM Atrophy and MS Disability. Ann Neurol 2014; 76: 568–80.

Shechter R, Miller O, Yovel G, Rosenzweig N, London A, Ruckh J, et al. Recruitment of beneficial m2 macrophages to injured spinal cord is orchestrated by remote brain choroid plexus. Immunity 2013; 38: 555–69.

Stilund M, Reuschlein A-K, Christensen T, Møller HJ, Rasmussen PV, Petersen T. Soluble CD163 as a marker of macrophage activity in newly diagnosed patients with multiple sclerosis. PLoS One 2014; 9: e98588.

Stoessel D, Stellmann J-P, Willing A, Behrens B, Rosenkranz SC, Hodecker SC, et al. Metabolomic profiles for primary progressive multiple sclerosis stratification and disease course monitoring. Front Hum Neurosci 2018; 12: 226.

Stroman PW, Wheeler-Kingshott C, Bacon M, Schwab JM, Bosma R, Brooks J, et al. The current state-of-the-art of spinal cord imaging: methods. Neuroimage 2014; 84: 1070–81.

Thompson AJ, Banwell BL, Barkhof F, Carroll WM, Coetzee T, Comi G, et al. Diagnosis of multiple sclerosis: 2017 revisions of the McDonald criteria. Lancet Neurol 2018; 17: 162–73.

Trapp DB, Vignos M, Dudman J, Chang A, Fisher E, Staugaitis SM, et al. Cortical neuronal densities and cerebral white matter demyelination in multiple sclerosis: a retrospective study. Lancet Neurol 2018; 17: 870–84.

Treaba CA, Granberg TE, Sormani MP, Herranz E, Ouellette RA, Louapre C, et al. Longitudinal characterization of cortical lesion development and evolution in multiple sclerosis with 7.0-T MRI. Radiology 2019; 291: 740–9.

Vidaurre OG, Haines JD, Katz Sand I, Adula KP, Huynh JL, McGraw CA, et al. Cerebrospinal fluid ceramides from patents with multiple sclerosis impair neuronal bioenergetics. Brain 2014; 137: 2271–86.

Vercellino M, Votta B, Condello C, Piacentino C, Romagnolo A, Merola A, et al. Involvement of the choroid plexus in multiple sclerosis autoimmune inflammation: a neuropathological study. J Neuroimmunol 2008; 199: 133–41.

Van der Walt S, Schönberger JL, Nunez-Iglesias J, Boulogne F, Warner JD, Yager N, et al. scikit-image: image processing in Python. PeerJ 2014; 2: e453.

Zhao W, Cohen-Adad J, Polimeni JR, Keil B, Guerin B, Setsompop K, et al. Nineteen-channel receive array and four-channel transmit array coil for cervical spinal cord imaging at 7T: RF Coil for Spinal Cord MRI at 7T. Magn Reson Med 2014; 72: 291–300.

Zurawski J, Lassmann H, Bakshi R. Use of magnetic resonance imaging to visualize leptomeningeal inflammation in patients with multiple sclerosis: a review. JAMA Neurol 2017; 74: 100–9.